RSC Advances

ROYAL SOCIETY OF CHEMISTRY

www.rsc.org/advances

A Single-beam-splitting Technique Combined with Calibration-free Method for Field-deployable Applications using Laser-induced Breakdown Spectroscopy

Mingjun Xu[a,b], Qingyu Lin[b], Guang Yang[b], Tao Xu[b], Tianlong Zhang[c], Xu Wang[b], Shuai Wang[b], Fang Bian[b], Yixiang Duan[b] *

[a]*College of Chemistry, Sichuan University, Chengdu 610064, China*

[b]*Research Center of Analytical Instrumentation, Key laboratory of bio-resource and eco-environment, ministry of education, College of Life Science, Sichuan University, Chengdu, 610064, China*

[c]*College of Chemistry and Materials Science, Northwest University, Xi'an 710069, China*

*Correspondence to: Dr. Yixiang Duan, Research Center of Analytical Instrumentation, College of Life Sciences, Sichuan University, Chengdu 610064, China

E-mail: yduan@scu.edu.cn Phone: 028-85418180 Fax: 028-85418180

Abstract:

In this work, a single-beam-splitting laser-induced breakdown spectroscopy (LIBS) technique using one single laser system is demonstrated. An individual pulse delivered by a laser (1064 nm wavelength) was split into two sub-pulses by a beam splitter. Various copper alloy standard disks were used in this investigation. Intensity enhancement of emission lines under different laser energies was investigated and the maximum enhancement of 2.1 was reached with 30 mJ laser energy. Under this optimal condition, quantitative analysis based on single-beam-splitting ablation with calibration-free (CF) method was performed and a better analytical result than that obtained based on single-pulse CF-LIBS was acquired. Combined internal reference for self-absorption correction (IRSAC) method and calibration-free inverse method, the analytical results agreed well with the certified values of the elements in the sample, with an accuracy error between -17% and +12%.

Key words: Laser-induced breakdown spectroscopy, Calibration-free method, A single-beam-splitting technique, Internal reference for self-absorption correction method, Calibration-free inverse method

1. *Introduction*

Laser-induced breakdown spectroscopy (LIBS) is a plasma technique based on atomic emission spectroscopy. Traditional LIBS (single-pulse LIBS) uses a high-powered laser pulse focusing on a sample. The sample material is heated, ablated, atomized and ionized, and ultimately formed a luminous plasma plume. Deductible quantitative and qualitative information of the sample can be acquired by analyzing the emission spectrum from the plasma. LIBS has many advantages, including fast multi-elemental analysis ability of virtually any kind of sample (solid, liquid, gas or aerosol), few sample preparation procedures, possibility of in situ and remote analysis[1-5], which have rendered it particularly suitable for field applications.

Single-pulse LIBS instruments have been adopted in field applications such as AvaLIBS. But they suffer from poor signal intensity and therefore relatively high limits of detection (1-100 ppm). However, a dual-pulse technique can enhance the sensitivity of LIBS obviously.[6-8] A dual-pulse LIBS system requires either a pair of laser systems or a single laser which can generate two time separated pulses.[9, 10] Using a dual-pulse LIBS system for stronger coupling of laser energy to the ablated target allows enhanced emission intensities, lower detection limits, stronger sustained plasma emission.[11] Therefore sharper and less self-absorption spectra are acquired. Signal enhancement in the dual-pulse LIBS system is consistently observed by many research groups.[6, 7, 12, 13] But dual-pulse LIBS technique is more expensive and more complex compared to the single-pulse LIBS technique, which hinders its field application. Alternatively, Antony et al. proposed and demonstrated a novel single laser based dual-wavelength ablation technique, which enables a compact instrument for field applications while maintaining the main advantages of dual-pulse LIBS mentioned above.[9] In this work, similarly, a novel single-beam-splitting method was adopted to enable a simple and low-cost instrument for field applications while maintaining the main advantages of

dual-pulse LIBS.

After obtaining excellent spectra with single-beam-splitting technique, practical quantitative analysis was required for field applications. Calibration-based method frequently used in LIBS is not a good choice since matrix-matched reference materials with a composition similar to the unknown sample are not accessible in most cases, especially in field applications. An alternative method, calibration-free (CF) method developed in 1999[14], offers another choice for realizing quantitative analysis in field applications. CF method is based on a complete optical diagnostic procedure of plasma. It is capable of determining elemental composition of sample materials without using calibration curves involving matrix-matched reference materials. CF method has been widely used to analyze plasmas of various samples (precious alloys[15], bronze alloys[16] , sludge[17], multi-component oxide materials[18] etc.) generated by single-pulse LIBS. CF method was also used to analyze plasmas of steel generated by dual-pulse LIBS. V. Contreras et al. used dual-pulse CF-LIBS to analyze plasma of steel sample.[19] Their results showed that quantitative analysis by dual-pulse CF-LIBS was slightly better than that by single-pulse CF-LIBS.

However, CF-LIBS analysis has not yet reached the diffusion that a standard-less LIBS technique could potentially obtain, especially in field applications.[20] The reason is that the accuracy of analysis results is unsatisfied. In order to improve CF-LIBS algorithm to obtain more accurate results, various methods were implemented in the CF-LIBS algorithm, including one-point calibration method[20], calibration-free inverse method[21], Curve of Growth (COG) method[22], and internal reference for self-absorption correction (IRSAC) method[23].

The aim of our current work is to use a single-beam-splitting LIBS technique to realize signal enhancement along with a CF algorithm for practical quantitative analysis, promoting LIBS techniques for field applications. In this work, an individual pulse delivered by a Q-switched Nd^{3+}:YAG laser was split into two sub-pulses by a beam splitter, which enabled a simple and low-cost system for field applications while maintaining the main advantages of dual-pulse LIBS. CF method was adopted to determine elemental composition of sample materials without using calibration curves

involving matrix-matched reference materials. Besides, calibration-free inverse method and IRSAC method were combined to improve the accuracy of CF method under this system for the first time, and a better result was obtained with such a combination.

2. Experimental

2.1 Instrumentation

The experimental setup used for our studies performed under atmospheric conditions is shown in Figure 1. An individual pulse delivered by a Q-switched Nd3+:YAG laser (Litron Lasers, LPU 450，wavelength λ = 1064 nm, a pulse duration $\tau_L \approx$ 6 ns, pulse energy $E_L \leqslant$ 120 mJ, repetition rate $f_r \leqslant$ 20 Hz) was split into two sub-pulses by a beam splitter (50:50). One sub-pulse was focused vertically onto a sample using a plano-convex lens (150 mm focal length). The other one was focused onto the same position of the sample using a plano-convex lens with short focal length (50 mm focal length) at about 30° with respect to the sample surface. We considered that the two sub-pulses arrived at the sample surface simultaneously since the optical path length difference can be neglected. The ablation laser spot on the surface of the sample was nearly circular and its diameter was measured to be about 300 μm. The emission from the plasma was collected through a collecting lens and it was fed to a three-channel spectrograph (Avantes, AvaSpec, Netherlands) with broadband covered a range of 200 – 940 nm (0.15 nm resolution). The detector was a linear CCD with 2048 pixels. A signal delay controller in the spectrograph was used to control the acquisition time settings via the AvaSoft 7.7 software. Single-pulse LIBS experiment was performed by removing the beam splitter for comparison with the single-beam-splitting LIBS experiment.

2.2 Sample preparation and data acquisition

For each surface of every sample cleaned by ethanol, 55 different locations were selected for measurement. A single shot per location was chose to obtain a measured spectrum to avoid sample destruction. To minimize the influence from sample

heterogeneity and other fluctuations, the 55 measured spectra at different locations were averaged into an analytical spectrum. In this experiment, the energy was monitored in real-time by an energy meter and all of the acquired spectra were dark current corrected using the AvaSoft 7.7 software.

The samples used in this study were copper alloy standard disks (BYG1916-1-3, BYG1916-1-4, BYG1916-1-5, BYG1916-1-6, BYG1916-1-7) from Southwest Aluminum of China. A description of the samples is given in Table 1 for elemental composition and quantitative information.

2.3 Quantitative analysis

Practical quantitative analysis was conducted with CF algorithm, which is more sensitive to the self-absorption effect with respect to the traditional calibration-based method.[22] In order to improve CF-LIBS algorithm to obtain more accurate results, internal reference for self-absorption correction (IRSAC) method was used to correct self-absorption effect and calibration-free inverse method was used to correct plasma temperature.

2.3.1 CF algorithm

CF algorithm was performed to realize quantitative analysis of our samples. Four assumptions should be fulfilled before using CF method in an experiment[24]: the plasma composition is representative of the unperturbed target composition, the plasma can be modeled as a spatially homogeneous source, and the plasma is optically thin and in LTE in the temporal and spatial observation window. Under these conditions, a plasma could be described by Maxwell–Boltzmann distribution and other equilibrium relations.[25] Boltzmann equation could be applied to determine the elemental composition of the ablated sample, expressed as:

$$\ln\left[I_{ki}^{\lambda}/(A_{ki}g_k)\right] = -E_k/(k_B T) + \ln\left[C_s F/U(T)\right] \qquad (2)$$

Here I_{ki}^{λ} is the measured integral line intensity of a spectral line of wavelength λ, g_k is the degeneracy of the upper level, the A_{ki} is Einstein coefficient of spontaneous

emission for the "ki" transition, k_B is Boltzmann constant, C_S is the relative concentration of emitting species, E_k is the upper level energy, U(T) is partition function for the emitting species, and F is an experimental parameter that takes into account the optical efficiency of the collection system as well as the total plasma number density and volume.[23]

To evaluate plasma temperature, Boltzmann plot of $\ln(I^{\lambda}_{ki}/A_{ki}*g_{k})$ vs E_k having slope of $(-1/k_BT)$ had to be drawn for every element present in a sample. The intercept of a Boltzmann plot can be related to the concentration of an element present in the sample. The intercept value, q_s, is a function of the concentration of the corresponding element present in the plasma. Since the sum of the relative concentration of all species equal unity, the experimental factor F can be determined using the following normalization relation,

$$\sum_{s} Cs = \frac{1}{F}\sum_{S} Us(T)e^{q_s} = 1 \qquad (3)$$

and the concentration of all the species in the sample can be obtained by

$$Cs = \frac{1}{F}Us(T)e^{q_s} \qquad (4)$$

In addition, because the calculation of plasma temperature affects both intercept value and partition function, Saha-Boltzmann method is used to draw a Saha-Boltzmann plot for obtaining a more reliable plasma temperature. In Saha-Boltzmann method, lines from atoms and ions of the same element are included in a linear regression equation thus improving the statistics[26]. Here Saha-Boltzmann method was not used because calibration-free inverse method was used to correct plasma temperature

Distinctly, CF method avoids the use of standard samples to get the calibration curve. Combine CF method with the single-beam-splitting technique, a practical field analysis method was expected.

2.3.2 Internal reference for self-absorption correction (IRSAC) method

Internal reference for self-absorption correction (IRSAC) method was proposed

by Lanxiang Sun.[23] An internal reference line for each species was chosen at first, then compared with other spectral line intensities of the same species to estimate the self-absorption degrees of other spectral lines, and finally achieved an optimal correction by a regressive algorithm. The self-absorption effect of the selected reference line can be ignored, since the reference line with high excitation energy of the upper level is slightly affected by the self-absorption. The corrected intensity of a spectral line is expressed as

$$\hat{I}_{\lambda}^{\mathrm{ki}} = \frac{I_{\lambda}^{ki}}{f_{\lambda}^{b}} = \frac{I_{\lambda_R}^{mn} A_{ki} g_k}{A_{mn} g_m} e^{(E_{\mathrm{m}} - E_k)/k_B T} \qquad (5)$$

Where $I_{\lambda_R}^{mn}$ and f_{λ}^{b} are the spectral line intensity and self-absorption coefficient of the internal reference line, and the A_{mn}, g_m and E_m are the spectral parameters related to the transition between energy levels of m and n.

2.3.3 Calibration-free inverse method

Calibration-free inverse method was proposed by R. Gaudiuso et al., based on the LTE equations.[27] It was applied to simulate the elemental composition of a certified sample at different temperatures, assuming that the actual plasma temperature was the one providing the best agreement with certified data. In addition, it introduces a further practical assumption, i.e., that if different samples with similar matrices are ablated in the same conditions, the excitation temperatures of the produced plasmas are the same.[21]

Figure-1

Table-1

3. Results and Discussion

3.1 Delay time for an optically thin and local thermodynamic equilibrium (LTE) plasma

In the process of plasma cooling, the plasma in a period of time meets the local thermal equilibrium (LTE) condition. Different particles in plasma have a common temperature T in LTE. Plasma in LTE can be described by Maxwell–Boltzmann distribution and other equilibrium relations[25], which is the basis of quantitative analysis. Therefore delay time was optimized to obtain the delay time where the plasma was optically thin (less self-absorption) as well as in LTE. If a plasma is optically thin and in LTE, the intensity ratio of two emission lines of the same species should be nearly the same as the ratio of the product of transition probability (A_{ki}), statistical weight (g_k), and inverse ratio of their wavelengths[28], i.e.:

$$I / I' = A_{\mathrm{ki}} g_k \lambda' / A_{ki}' g_k' \lambda \qquad (1)$$

Here the two emission lines have the same or close upper level.

Sample BYG1916-1-4 was chose to optimize delay time. A pulse energy of 24mJ was used which provided a calculated incident laser irradiance of 5.66×10^9 W/cm^2. Stoichiometric ablation of the sample was fulfilled at this condition.[29] The delay time where the plasma was optically thin and in LTE was inferred from the temporal evolution of the intensity ratio of two Cu I lines (515.32 and 521.82 nm) and two Al I lines (308.21 and 309.27 nm) when laser energy was 24mJ (Figure 2). Peak intensity was baseline corrected by off peak background correction method. The intensity ratios for two Cu I lines (515.32 and 521.82 nm) and two Al I lines (308.21 and 309.27 nm) using eq. (1) were equal to 1.75 and 1.80, respectively. Comparing the experimental data of the intensity ratio with the theoretical one, we found intensity ratios were in close agreement with 1~6% variation with the theoretical values obtained when the delay time was 0.64 μs.

Figure-2

3.2 Intensity Enhancement of Spectral Lines

Entire enhancement in the LIBS signal was observed at the pulse energy of 24 mJ and the delay time of 0.64 μs. To compare with single pulse LIBS, as shown in Figure 3, the signal enhancements of neutral and ionic species of the sample

BYG1916-1-4 were obvious. Different emission lines in the plasma showed different intensity enhancement factors and a maximum of 1.8-fold enhancement was obtained for the Cu II line at 213.60 nm. Here intensity enhancement factor was defined as the ratio between the intensity with single-beam-splitting excitation and intensity with single-pulse excitation. Each used spectral line was baseline corrected.

For laser-induced plasma on a plane surface and expanding up the laser beam, there were three important zones: the plasma front, the shock front and the absorption front. The absorption front zone come up just behind the shock front, and both were ahead of the plasma front.[30] In this experiment, one pulse with 24mJ energy was split into two same sub-pulses with different incident angles. The absorption front of the plasma expanded, providing more energy for the plasma front zone and obtaining effective pulse–plasma energetic coupling.[31] The shock front would become thin because of energy dispersion, reducing shielding for spectral signal emission. Consequently, spectral line-intensity enhancement was observed.

Table 2 shows enhancement factors of different emission lines in the plasma for different ns-laser pulse energies in the single-beam-splitting experiment. Except for Mn II (257.61 nm), the enhancements of other emission lines reached maximum when the laser energy was 30 mJ. We considered that the absorption front zone further expanded and the shock front became thick gradually with the increase of the laser energy. When the thickness of the shock front of the plasma in the single-beam-splitting LIBS was similar to that in single-pulse LIBS, signal enhancement was not observed.

Plasma temperature and electron density in single-beam-splitting LIBS experiment were calculated under different ns-laser pulse energies. The plasma temperature was calculated from Boltzmann plots of Cu I lines and Al I lines. Since Cu and Al were abundant in our sample, a lot of Cu and Al atomic lines could be found to make accurate Boltzmann plots. The temperature values obtained for the different sample constituents were different due to self-absorption effect. The temperature values calculated from Cu and Al atomic constituents of the target were averaged as plasma temperature of the sample BYG1916-1-4. The electron density was calculated from

Stark broadening of Al I line at 309.27 nm. In order to obtain the Stark broadening, Voigt function was used to fit the Al I line at 309.27 nm, and then the instrumental broadening component was deconvoluted. In this experimental condition, the instrumental broadening approximated to 0.055 nm. Calculated results were compared to those in single-pulse LIBS (Table 3). Comparing the experimental data of the single-beam-splitting LIBS with that of single-pulse LIBS, temperatures were in close agreement. Temperature further expanded with increased ns-laser pulse energies. The electron density in the single-beam-splitting LIBS increased compared to that in single-pulse LIBS under 24 mJ and 30 mJ. It demonstrated that effective pulse–plasma energetic coupling existed in the single-beam-splitting LIBS under low energy. The increasing of electron density in the single-beam-splitting LIBS compared to single-pulse LIBS further decreased with the increasing of ns-laser pulse energies. It demonstrated that signal enhancement was partly attributed to the shock front's attenuation because of energy dispersion. Therefore, effective pulse–plasma energetic coupling and shock front's attenuation were the main reasons for signal enhancement.

Figure-3

Table-2

Table-3

3.3 Quantitative analysis based on single-beam-splitting LIBS with CF method

3.3.1 Quantitative analysis of sample BYG1916-1-6 with CF method

To evaluate quantitative analysis based on the single-beam-splitting technique with CF method, sample BYG1916-1-6 was analyzed at first. The wide wavelength range spectrum from 197 to 945 nm of the sample was recorded at a delay time of 0.64 μs and a pulse energy of 30 mJ. The pulse energy of 30 mJ provided a calculated incident laser irradiance of 7.07×10^{9} W/cm^{2}. Stoichiometric ablation of the sample was

fulfilled at this condition.[29] The delay time of 0.64 μs was the time when a optically thin and LTE plasma appeared in our experiment. 91 spectral lines from 4 different elements (Al, Cu, Fe and Mn) found were used to perform CF algorithm for sample BYG1916-1-6 (Table 4). CF analysis used in this section did not correct for self-absorption effects. Relevant spectral information—such as ionization energy values for each element, upper and lower level energies, or transitions probabilities for each line—was taken from the atomic spectral line database of Harvard University.

Electron density was determined using the Stark width of Al I line at 309.27 nm, too. The electron number density obtained was 2.1×10^{17} cm^{-3} for the sample analyzed. In order to prove the existence of LTE in the plasma at the delay time of 0.64 μs, we calculated the lower limit of the electron density according to McWhirter criterion. The result was 1.2×10^{16} cm^{-3}, which clearly demonstrated that the plasma was in LTE at the delay time of 0.64 μs and equation (1) was effective to find a plasma in LTE. The plasma temperature was calculated from Boltzmann plots of Cu I lines and Al I lines as mentioned before. We averaged the temperature values calculated from Cu and Al atomic constituents of the target as plasma temperature of the sample BYG1916-1-6. The plasma temperature was 12845.9 K. Plasma temperature and electron number density for single-pulse LIBS were calculated for comparison, which were equal to 11605.7 K and 2.0×10^{17} cm^{-3}.

The results of the calibration-free analysis of sample BYG1916-1-6 was reported in Table 5. CF analysis based on single-beam-splitting technique (SBS CF-LIBS in table 5) was compared to that based on single-pulse LIBS (Basic CF-LIBS in table 5). For Al in the sample, obvious underestimation of its relative concentration appeared in basic CF-LIBS. This was attributed to self-absorption effect. The quantitative result of Al affected the results of other elements, because the sum of the relative concentrations of all elements was equal to one in CF algorithm.

Energy dispersion in single-beam-splitting LIBS alleviated self-absorption effect, therefore, quantitative result of Al was close to the standard value. Generally speaking, quantitative results based on the single-beam-splitting technique were better than

those based on single-pulse LIBS, which could be attributed to less self-absorption effect and shaper spectra in the single-beam-splitting LIBS. However, the calculated relative errors of the four elements in sample BYG1916-1-6 were not satisfied (3%~25%). The reasons were that self-absorption effect was not deducted and the uncertainties associated with temperature determination as well as intensity fluctuations. Quantitative analysis based on single-beam-splitting LIBS with a modified CF method was performed in next section.

Table-4

Table-5

3.3.2 Quantitative analysis based on the single-beam-splitting LIBS along with a modified CF algorithm

Combined IRSAC method with CF inverse method in calibration free analysis was used to improve calibration free analysis of sample BYG1916-1-6 based on single-beam-splitting LIBS system. Then quantitative analysis based on the single-beam-splitting LIBS along with this modified CF algorithm was applied to analyze other samples. Selected analytical lines for all samples are listed in Table 4. The boldfaced numbers in table 4 represent the selected reference lines.

IRSAC method was used to correct spectral line intensity of the four elements in sample BYG1916-1-6. The plasma temperature in equation (5) was preliminarily evaluated from the Boltzmann plots of Cu I and Al I without any correction. The Boltzmann plots of the four elements in sample BYG1916-1-6, determined by the basic CF-LIBS method and IRSAC method, are shown in Figure 4 (a~h). Before correction, the points on Boltzmann plots very scattered because of self-absorption effect. The self-absorption effect causes their plasma temperature calculated higher than real values, the intercepts lower than expected, and finally large errors in the quantitative results.[23] It was clear that scattered points on the Boltzmann plots were corrected effectively with IRSAC method, improving intercepts estimation.

We used Boltzmann plots corrected by the IRSAC for sample BYG1916-1-6 to

perform CF algorithm. The results were listed in forth column of Table 6, far away from standard values. Intercept, related to the concentration of corresponding element present in the sample, was corrected by IRSAC method. The deviation of calculated CF results was possibly caused by temperature. Subsequently, we reduced the plasma temperature and calculated CF results of the sample BYG1916-1-6 with four different reduced temperatures. It demonstrated that when the plasma temperature was 8905.9K, the relative error of relative concentration of the sample BYG1916-1-6 was minimum (-15%~12%). Quantitative analysis results improved significantly.

CF inverse method assumed that the actual plasma temperature was the one providing the best agreement with certified data. Therefore, 8905.9K was the actual plasma temperature of the sample BYG1916-1-6 according to CF inverse method. In addition, CF inverse method introduces a further practical assumption, i.e., that if different samples with similar matrices are ablated in the same conditions, the excitation temperature of the produced plasmas is the same. In our experiment, the five samples were similar no matter in components or in element content. So we used 8905.9K as the plasma temperature of other samples. BYG1916-1-3, BYG1916-1-4, BYG1916-1-5, BYG1916-1-7 were analyzed by CF algorithm as well. We corrected Boltzmann plots of different species in the corresponding sample with IRSAC method using temperature of 8905.9K. All results were listed in column 6 of Table 7. They were compared with results of basic CF method and CF method based on single-beam-splitting LIBS. It was clear that with the combined IRSAC method and calibration-free inverse method, the analytical results agreed well with the certified values of the elements in the sample. For Cu in the standard samples, the relative errors obtained were between -1.5% and +1.5%. For other elements, the relative errors obtained were between -17% and 12%. The reliability of quantitative analysis was significantly improved.

Figure-4

Table 6

Table 7

Conclusions

A novel beam-splitting method was demonstrated in this work. An individual pulse delivered by the laser was split into two sub-pulses by a beam splitter, which enabled a simple and low-cost system for field applications while maintaining the main advantages of dual-pulse LIBS. CF analysis based on this system was evaluated. IRSAC method and calibration-free inverse method were combined to improve CF analysis for the first time. The analytical results agreed well with the certified values of the elements in the sample, with an accuracy error between -17% and +12%. The reliability of quantitative analysis was improved in our method with only one matrix-matched reference material. Applied improved CF analysis with a single-beam-splitting LIBS system for practical field analysis was expected.

Acknowledgement

The authors are grateful to the financial support from the National Major Scientific Instruments and Equipments Development Special Funds (No. 2011YQ030113), the National Recruitment Program of Global Experts (NRPGE), the Hundred Talents Program of Sichuan Province (HTPSP), and the Startup Funding of Sichuan University for setting up the Research Center of Analytical Instrumentation.

Reference

1. Kaiser, J., et al., *Trace elemental analysis by laser-induced breakdown spectroscopy—Biological applications.* Surface Science Reports, 2012. **67**(11-12): p. 233-243.
2. Gobernado-Mitre, I., et al., *On-line monitoring of laser cleaning of limestone by laser-induced breakdown spectroscopy and laser-induced fluorescence.* Applied spectroscopy, 1997. **51**(8): p. 1125-1129.
3. Zhu, X., et al., *Advanced statistical analysis of laser-induced breakdown spectroscopy data to discriminate sedimentary rocks based on Czerny–Turner and Echelle spectrometers.* Spectrochimica Acta Part B: Atomic Spectroscopy, 2014. **93**: p. 8-13.
4. Gehlen, C.D., et al., *Chlorine detection in cement with laser-induced breakdown spectroscopy in the infrared and ultraviolet spectral range.* Spectrochimica Acta Part B: Atomic Spectroscopy, 2009. **64**(10): p. 1135-1140.
5. Wilsch, G., et al., *Determination of chloride content in concrete structures with laser-induced breakdown spectroscopy.* Construction and Building Materials, 2005. **19**(10): p. 724-730.

6. Babushok, V.I., et al., *Double pulse laser ablation and plasma: Laser induced breakdown spectroscopy signal enhancement.* Spectrochimica Acta Part B: Atomic Spectroscopy, 2006. **61**(9): p. 999-1014.
7. Cavalcanti, G.H., et al., *Double-pulse laser-induced breakdown spectroscopy analysis of scales from petroleum pipelines.* Spectrochimica Acta Part B: Atomic Spectroscopy, 2013. **87**: p. 188-191.
8. Rai, V.N., F.-Y. Yueh, and J.P. Singh, *Study of laser-induced breakdown emission from liquid under double-pulse excitation.* Applied optics, 2003. **42**(12): p. 2094-2101.
9. Antony, J.K., et al., *Single laser based dual-wavelength ablation technique for emission enhancement during LIBS.* Journal of Physics D: Applied Physics, 2012. **45**(36): p. 365401.
10. Guo, J., et al., *Emission enhancement ratio of the metal irradiated by femtosecond double-pulse laser.* Optics Communications, 2012. **285**(7): p. 1895-1899.
11. Choi, S.J. and J.J. Yoh, *Effective laser-induced breakdown spectroscopy (LIBS) detection using double pulse at optimum configuration.* Appl Spectrosc, 2011. **65**(8): p. 952-6.
12. Stratis, D.N., K.L. Eland, and S.M. Angel, *Dual-pulse LIBS using a pre-ablation spark for enhanced ablation and emission.* Applied Spectroscopy, 2000. **54**(9): p. 1270-1274.
13. Gondal, M.A., et al., *Detection of sulfur in the reinforced concrete structures using a dual pulsed LIBS system.* Optics & Laser Technology, 2012. **44**(3): p. 566-571.
14. Ciucci, A., et al., *New procedure for quantitative elemental analysis by laser-induced plasma spectroscopy.* Applied Spectroscopy, 1999. **53**(8): p. 960-964.
15. Corsi, M., et al., *A fast and accurate method for the determination of precious alloys caratage by Laser Induced Plasma Spectroscopy.* European Physical Journal D, 2001. **13**(3): p. 373-377.
16. Colao, F., et al., *LIBS as a diagnostic tool during the laser cleaning of copper based alloys: experimental results.* Journal of Analytical Atomic Spectrometry, 2004. **19**(4): p. 502-504.
17. Kumar, R., et al., *Monitoring of toxic elements present in sludge of industrial waste using CF-LIBS.* Environmental monitoring and assessment, 2013. **185**(1): p. 171-180.
18. Pedarnig, J.D., et al., *Element analysis of complex materials by calibration-free laser-induced breakdown spectroscopy.* Applied Physics A, 2012. **112**(1): p. 105-111.
19. Contreras, V., et al., *Double-pulse and calibration-free laser-induced breakdown spectroscopy at low-ablative energies.* Optics letters, 2012. **37**(22): p. 4591-4593.
20. Cavalcanti, G.H., et al., *One-point calibration for calibration-free laser-induced breakdown spectroscopy quantitative analysis.* Spectrochimica Acta Part B: Atomic Spectroscopy, 2013. **87**: p. 51-56.
21. Gaudiuso, R., et al., *Laser-induced breakdown spectroscopy of archaeological findings with calibration-free inverse method: Comparison with classical laser-induced breakdown spectroscopy and conventional techniques.* Analytica Chimica Acta, 2014. **813**: p. 15–24.
22. Bulajic, D., et al., *A procedure for correcting self-absorption in calibration free-laser induced breakdown spectroscopy.* Spectrochimica Acta Part B, 2002. **57**: p. 339–353.
23. Sun, L. and H. Yu, *Correction of self-absorption effect in calibration-free laser-induced breakdown spectroscopy by an internal reference method.* Talanta, 2009. **79**(2): p. 388-95.
24. Tognoni, E., et al., *Calibration-Free Laser-Induced Breakdown Spectroscopy: State of the art.* Spectrochimica Acta Part B, 2010. **65**: p. 1-14.
25. Hahn, D.W. and N. Omenetto, *Laser-induced breakdown spectroscopy (LIBS), part I: review of basic diagnostics and plasma–particle interactions: still-challenging issues within the*

analytical plasma community. Applied spectroscopy, 2010. **64**(12): p. 335A-366A.

26. Tognoni, E., et al., *A numerical study of expected accuracy and precision in Calibration-Free Laser-Induced Breakdown Spectroscopy in the assumption of ideal analytical plasma.* Spectrochimica Acta Part B: Atomic Spectroscopy, 2007. **62**(12): p. 1287-1302.
27. Gaudiuso, R., et al., *Laser-induced plasma analysis of copper alloys based on Local Thermodynamic Equilibrium: An alternative approach to plasma temperature determination and archeometric applications.* Spectrochimica Acta Part B: Atomic Spectroscopy, 2012. **74-75**: p. 38-45.
28. UNNIKRISHNAN, V.K., et al., *Measurements of plasma temperature and electron density in laser-induced copper plasma by time-resolved spectroscopy of neutral atom and ion emissions.* Pramana -J. Phys., 2010. **74**(6): p. 983-993.
29. Burakov, V.S. and S.N. Raikov, *Quantitative analysis of alloys and glasses by a calibration-free method using laser-induced breakdown spectroscopy.* Spectrochimica Acta Part B: Atomic Spectroscopy, 2007. **62**(3): p. 217-223.
30. Radziemski, L.J. and D.A. Cremers, *Handbook of Laser Induced Breakdown Spectroscopy*, 2006, John Wiley & Sons, West Sussex, England.
31. Scaffidi, J., S.M. Angel, and D.A. Cremers, *Emission enhancement mechanisms in dual-pulse LIBS.* Analytical chemistry, 2006. **78**(1): p. 24-32.

List of tables

List of figures

elements in sample BYG1916-1-6 (a, c , e, g). Boltzmann plot corrected by the IRSAC for sample BYG1916-1-6 (b, d, f, h).

Figure 1 Schematic representation of single laser based dual-pulse LIBS experimental setup.

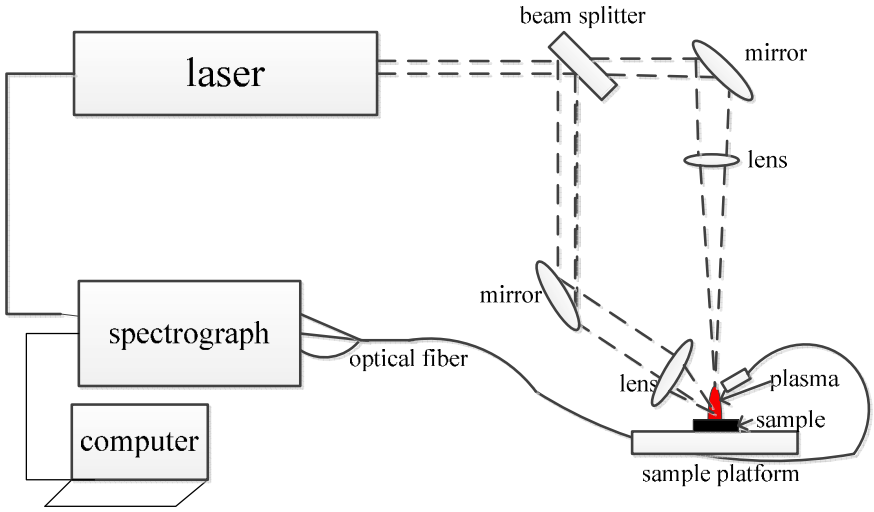

Figure 2. (a):Temporal evolution of intensities of two Cu I lines (515.32 and 521.82 nm) and their intensity ratio in single-beam-splitting LIBS experiment (24 mJ). (b): Temporal evolution of intensities of two Al I lines (308.21 and 309.27 nm) and their intensity ratio in single-beam-splitting LIBS experiment (24 mJ).

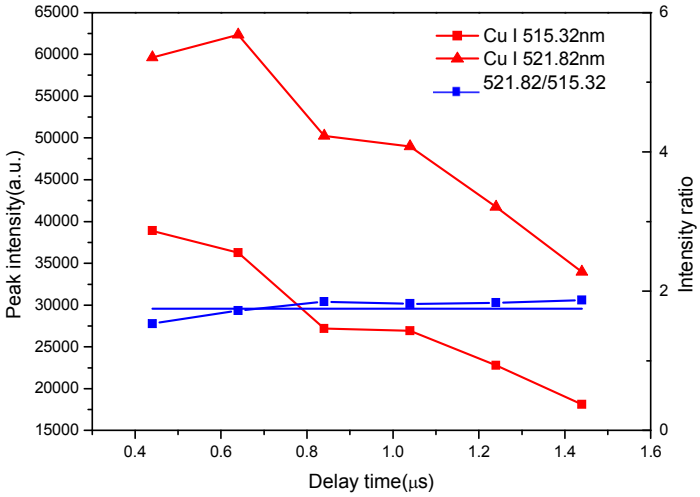

(a)

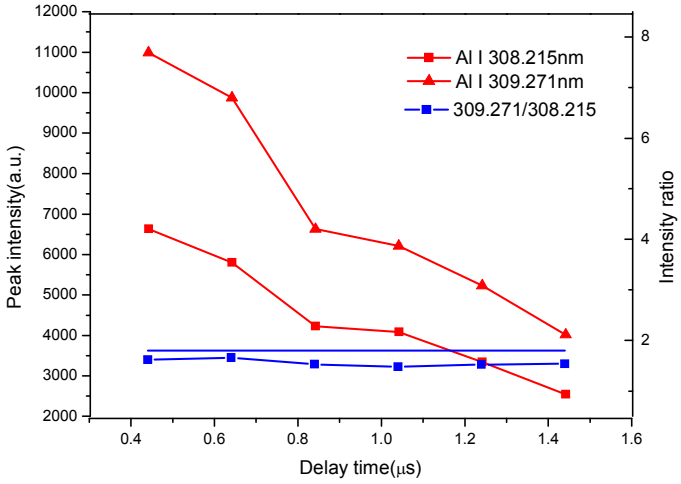

(b)

Figure 3. Spectra of the sample BYG1916-1-4 during single-pulse and single-beam-splitting LIBS experiments. The spectrum corresponding to a single pulse of 1064 nm with energy 24 mJ is shown by black. The spectrum corresponding to single-beam-splitting LIBS with energy 24mJ is shown by red. The delay time was 0.64 μs for both experiments.

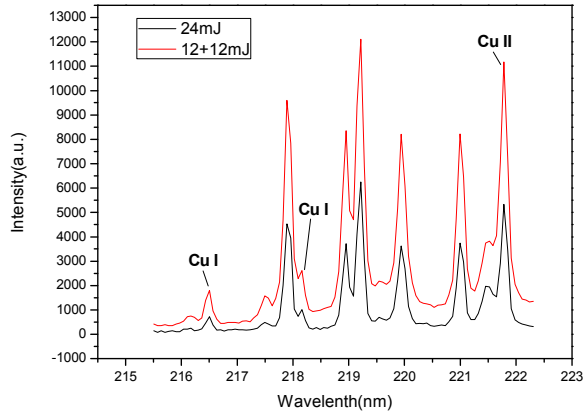

(a)

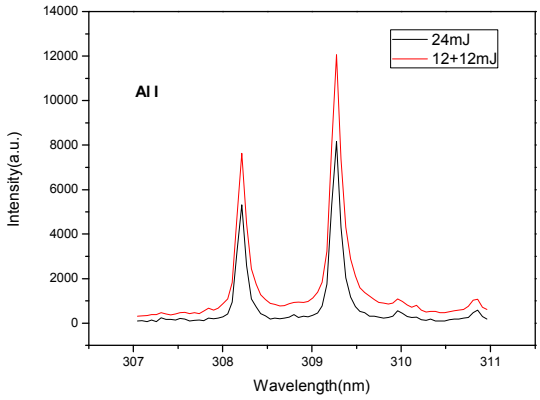

(b)

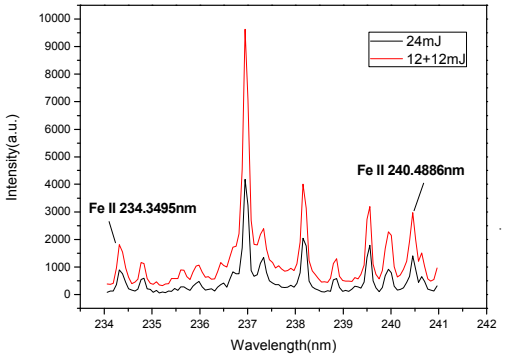

(c)

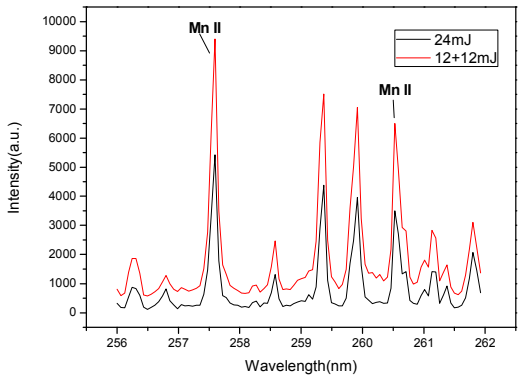

(d)

Figure 4 Initial Boltzmann plot derived from the raw line intensity of the four elements in sample BYG1916-1-6 (a, c , e, g). Boltzmann plot corrected by the IRSAC for sample BYG1916-1-6 (b, d, f, h).

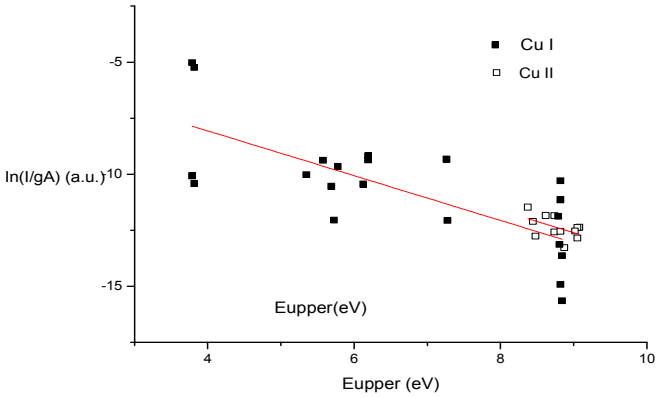

(a)

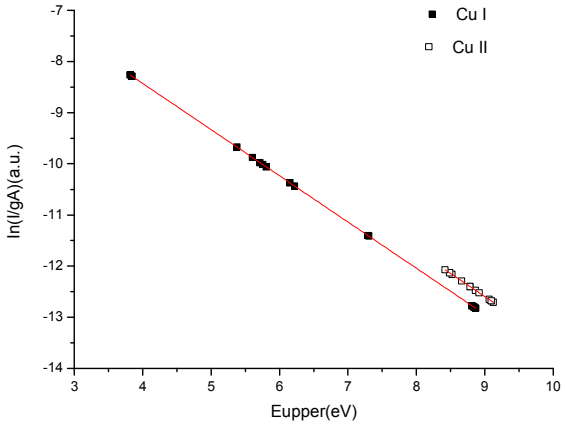

(b)

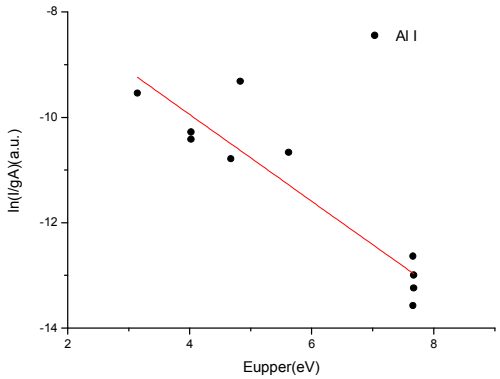

(c)

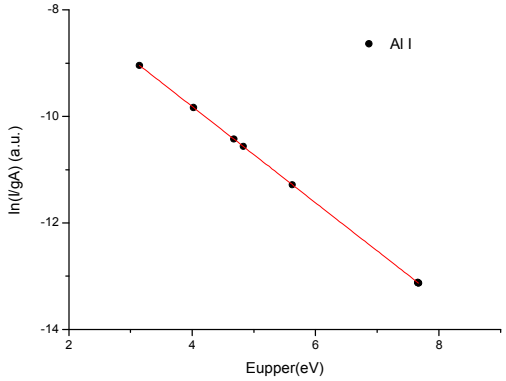

(d)

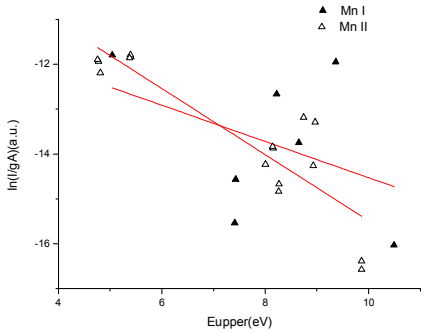

(e)

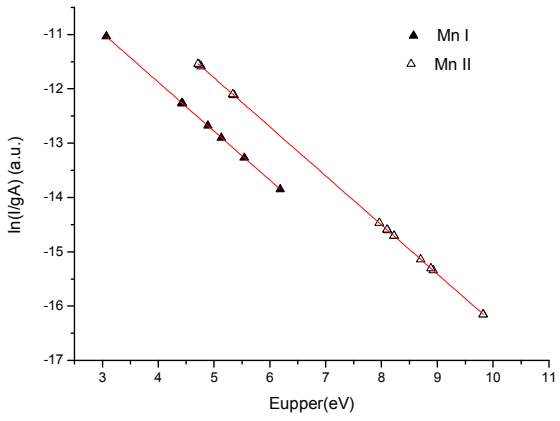

(f)

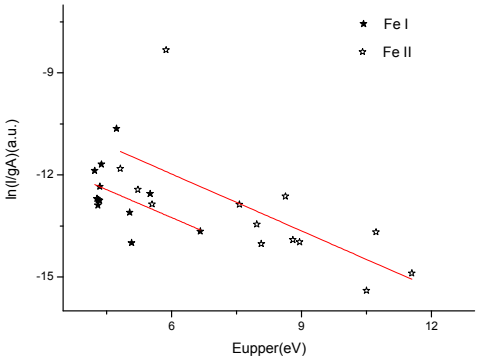

(g)

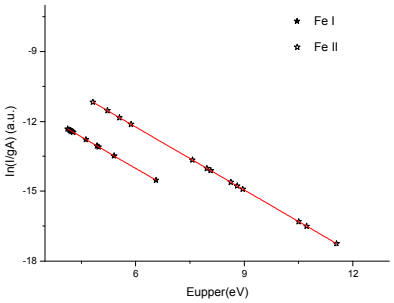

(h)

Table 1 Elemental percentage composition of copper alloy standards from Southwest Aluminum of China

	BYG1916-1-3	BYG1916-1-4	BYG1916-1-5	BYG1916-1-6	BYG1916-1-7
Cu	84.99	84.52	84.67	84.13	84.73
Al	9.24	9.14	7.76	8.78	9.75
Mn	1.56	1.57	2.63	2.92	2.01
Fe	3.01	3.17	4.94	4.17	3.51
Zn	0.69	1.11	0	0	0
other elements	0.51	0.49	0	0	0

Table 2. Signal enhancement under different laser energy.

		Enhancement factor		
Line	Wavelength(nm)	$I_{(12+12)mJ}/I_{24mJ}$	$I_{(15+15)mJ}/I_{30mJ}$	$I_{(18+18)mJ}/I_{36mJ}$
Cu II	213.60	1.80	2.10	1.23
Cu I	217.89	1.75	2.05	1.16
Al I	308.22	1.34	1.42	0.96
Fe II	234.35	1.34	1.78	0.55
Mn II	257.61	1.68	1.39	0.96

Table 3 Plasma temperature and electron density in single pulse LIBS and single laser based dual-pulse LIBS under different ns-laser pulse energies.

Experiment	Plasma temperature (K)	Electron density (cm^{-3})
Single pulse LIBS (24mJ)	11935.36	1.90×10^{17}
Single laser based dual-pulse LIBS (12+12mJ)	12405.35	2.44×10^{17}
Single pulse LIBS (30mJ)	11888.61	1.87×10^{17}
Single laser based dual-pulse LIBS (15+15mJ)	12693.13	2.12×10^{17}
Single pulse LIBS (36mJ)	13753.46	2.46×10^{17}
Single laser based dual-pulse LIBS (18+18mJ)	14834.45	2.11×10^{17}

Table 4 List of spectral lines used for building the Boltzmann plots for our copper-based alloy samples.

Species	Wavelength (nm)							
Cu I	216.5096	217.8949	261.8364	282.4365	296.1162	312.61	324.7537	327.3954
	329.0539	330.7945	356.6127	**364.838**	382.0875	386.046	510.5537	515.323
	521.8197	578.2127	809.2631	219.9754	359.9127			
Cu II	204.3802	205.4979	211.21	212.298	212.6044	213.5981	219.2268	212.8108
	224.2618	203.5854	199.9698	**197.9956**				
Al I	**221.006**	257.5094	265.2475	308.2153	309.271	394.4006	305.0072	305.4679
	305.7144	306.6144						
Mn I	279.4817	280.1081	**403.4483**	306.6028	476.5846	478.3427	602.1819	
Mn II	257.6105	259.3724	260.5684	293.3055	**293.9308**	294.9205	245.2487	243.7366
	249.9002	253.3324	254.875	255.6573	255.8606	261.8147	262.5611	270.1698
Fe I	296.6898	297.3235	299.4427	**302.0639**	304.7604	396.9257	297.3132	300.0948
	305.7446	306.7244	382.4306	489.1492				
Fe II	259.3728	262.549	232.6358	235.9113	**237.3736**	240.4982	253.8205	254.8744
	263.1048	266.6637	270.399	271.4413	317.9503			
Zn I	213.8573	**330.2584**	334.5015	481.0528	472.2153	468.0134	330.2941	328.2328
Zn II	206.2004	**209.9937**	255.7948	202.5483	250.1989			

Table 5 Quantitative results for sample BYG1916-1-6 in our work.

Sample	Element	Relative Concentration (wt%)			Relative Error (%)	
		Standard value	Basic CF-LIBS	SBS CF-LIBS	SBS CF-LIBS	
BYG1916-1-6	Cu	84.13	88.37	86.34	2.63	
	Al	8.78	3.53	8.04	-8.42	
	Mn	2.92	2.64	2.20	-24.55	
	Fe	4.17	5.46	3.41	-18.19	

Table.6 Relative concentrations of sample BYG1916-1-6 under different temperatures.

Sample	Element	Relative Concentration (wt%)						Relative Error (%)
		Standard value	12845.9K	9845.9K	9045.9k	8905.9K	8855.9K	8905.9K
BYG1916-1-6	Cu	84.13	56.28	76.78	82.66	83.65	84.00	-0.57
	Al	8.78	19.07	12.75	10.27	9.82	9.66	11.85
	Mn	2.92	10.47	4.10	2.70	2.48	2.41	-14.98
	Fe	4.17	14.18	6.37	4.37	4.05	3.93	-2.93

Table 7 Quantitave analysis results of sample BYG1916-1-7, BYG1916-1-5, BYG1916-1-4, BYG1916-1-3.

Sample	Element	Relative Concentration (wt%)				Relative Error(%)
		Standard value	Basic CF-LIBS	dual	new	new
BYG1916-1-7	Cu	84.73	93.51	85.53	85.61	1.28
	Al	9.75	3.05	11.16	9.63	5.34
	Mn	2.01	1.71	1.26	1.72	9.34
	Fe	3.51	1.74	2.05	3.05	-3.81
BYG1916-1-5	Cu	84.67	89.91	83.46	83.63	-1.23
	Al	7.76	3.36	9.41	8.42	8.46
	Mn	2.63	3. 03	1.59	2.43	-7.71
	Fe	4.94	3.70	5.53	5.52	11.83
BYG1916-1-3	Cu	84.99	89.69	86.43	84.41	-0.68
	Al	9.24	3.35	7.67	10.21	10.46
	Mn	1.56	3.02	1.43	1.39	-10.67
	Fe	3.01	3.69	3.37	3.41	-13.25
	Zn	0.69	0.25	1.10	0.58	-16.32
	Other elements					
BYG1916-1-4	Cu	84.52	93.36	88.00	84.31	-0.25
	Al	9.14	2.43	7.92	9.68	5.91
	Mn	1.57	1.25	1.20	1.53	-2.50
	Fe	3.17	2.95	1.97	3.53	11.41
	Zn	1.11	0.36	0.90	0.95	-14.56
	Other elements					